Gap Winds and their effects on regional oceanography Part I: Cross Sound, Alaska

Submitted to Deep Sea Research II

Carol Ladd[1] and Wei Cheng[2]

[1]Corresponding Author:
Carol Ladd
Pacific Marine Environmental Laboratory, NOAA
7600 Sand Point Way Seattle, WA, USA 98115-6349
Tel: (206) 526-6024
Fax: (206) 526-6485
Email: carol.ladd@noaa.gov

[2]Joint Institute for the Study of the Atmosphere and Ocean,
University of Washington, 3737 Brooklyn Ave NE, Box 355672,
Seattle, WA 98105-5672 USA
Email: wei.cheng@noaa.gov

Abstract

Gap-wind events flowing from Cross Sound in the eastern Gulf of Alaska (GOA) were examined using QuikSCAT wind data. The average duration of an event is 3.6 days with the longest event recorded in the QuikSCAT dataset being 12 days. Daily offshore directed winds with speeds > 10 m s^{-1} are more common during the winter months (October – March), averaging 20.0 days per year, and less common during the summer (April – September), averaging 2.8 days per year. Interannual variability in the frequency of gap-wind events is correlated with El Niño. During gap-wind events, the spatial scales of high off-shore directed winds (> 10 m s^{-1}) reach almost 200 km off-shore and 225 km along the shelf break, suggesting that the winds directly influence both the shelf (20 – 65 km wide) and the off-shore waters. A model experiment suggests that a gap-wind event can result in eddy formation and changes in circulation and water properties. Increased entrainment of water from below the mixed layer due to the gap-wind event implies that mixed-layer nitrate concentrations could increase on the order of 5 – 10 μmole/l, potentially enhancing primary production in the region. An accompanying paper discusses part II of our study (Ladd et al., this issue) focusing on gap-wind events in the western GOA around Kodiak Island.

1 Introduction

Winter storms in the North Pacific typically form east of Japan and cross the Pacific toward the Gulf of Alaska (GOA) (Rodionov et al., 2007; Rodionov et al., 2005; Wilson and Overland, 1986). The rugged, mountainous coastline of the GOA can interact with these synoptic-scale disturbances, resulting in strong coastal pressure gradients and gale force winds. In addition, the contrast between relatively warm offshore water and cold continental air over Alaska during winter results in strong hydrostatic pressure gradients along the coast (Macklin et al., 1988). The resulting coastal wind field can manifest as barrier jets, gap winds, downslope winds, and interactions between them (i.e. Loescher et al., 2006; Winstead et al., 2006; Young and Winstead, 2004).

Gap winds, defined here as offshore-directed flow channeled through mountain gaps, have been examined in a number of observational and modeling studies, beginning with Reed's (1931) study of strong winds blowing out of the Strait of Juan de Fuca (~54°N, 130°W). Since that time, gap winds have been examined in many regions around the world. In the GOA, Synthetic Aperture Radar (SAR) data have shown strong gap winds in Prince William Sound (Liu et al., 2008), flowing out of Iliamna Lake northeast of Kodiak Island (Ladd et al., this issue; Liu et al., 2006), and flowing out of Cross Sound in southeastern Alaska (Loescher et al., 2006; Winstead et al., 2006). Loescher et al. (2006) examined the climatology of coastal barrier jets in the GOA from SAR images. They divided the wind jets into two categories: classic barrier jets fed by onshore flow and jets fed by gap flow from the continental interior. They found that most of these wind jets occurred during the cool season, with gap-wind jets commonly found at the outflows of Cross Sound, Yakutat Bay, and Icy Bay in the eastern GOA (Fig. 1).

While gap winds and the conditions leading to them have been relatively well-described, their influence on the coastal ocean has been examined in only a few regions. Perhaps the most complete description of gap winds and their influence has been in the northeastern tropical Pacific. The gap winds associated with three mountain gaps in Central America have been shown to influence regional ocean circulation (Kessler, 2006), eddy formation (e.g. McCreary et al., 1989; Trasviña et al., 1995), and chlorophyll-*a* distributions (McClain et al., 2002). Liang et al. (2009) used satellite data to quantify the magnitude, duration and timing of anomalous ocean conditions associated with gap-wind events in this region.

Due to programs like GLOBEC Northeast Pacific (Batchelder and Bond, 2009) and NOAA's EcoFOCI (www.ecofoci.noaa.gov), the biology and physical oceanography of the western GOA (west of ~145°W) has been relatively well-studied (Fig. 1). However, the eastern GOA is not as well sampled. Circulation in the GOA includes the cyclonic subarctic gyre in the basin and the Alaska Coastal Current on the continental shelf (Fig. 1). The eastern boundary current of the subarctic gyre is the broad and variable Alaska Current. Eddies are regularly formed in the Alaska Current, with important consequences for fluxes of physical and chemical properties and biota (e.g. Atwood et al., 2010; Janout et al., 2009;

Ladd et al., 2009; Ladd et al., 2007; Okkonen et al., 2003). At the head of the gulf, the gyre turns southwestward to form the Alaskan Stream, a western boundary current, tightly confined to the shelf-break. The Alaska Coastal Current, a baroclinic coastal current driven by winds and freshwater, has been well described in the northern and western GOA (e.g. Kowalik et al., 1994; Royer, 1981; Schumacher and Reed, 1986; Stabeno et al., 2004; Stabeno et al., this issue-a). It has been described as part of a system of fresh water driven coastal flow extending from the Columbia River in Washington State, along the coast of British Columbia and Alaska, all the way into the Bering Sea (Kowalik et al., 1994). However, the properties and continuity of this coastal current in the *eastern* GOA have not been well studied (Weingartner et al., 2009). South of Cross Sound, the shelf is narrow (~20 km wide). The shelf is interrupted by Yakobi Sea Valley (> 200 m deep) at the exit of Cross Sound. North of the sea valley, the shelf is much wider (>65 km). Recent data collected in the eastern GOA finally allow a description of the coastal flow in this under-studied region, suggesting that the Alaska Coastal Current is not continuous across the Yakobi Sea Valley (Stabeno et al., this issue-b). This eastern GOA region is important for transportation, tourism, and fishing, and high winds can be treacherous to these industries. Thus it is important to understand the frequency and magnitude of gap-wind events in this under-studied region, and their impact on the regional oceanography.

Part I of our study focusses on gap winds flowing out of Cross Sound in the eastern GOA (Fig. 1). The focus of Part II of this study (Ladd et al., this issue) is on gap-wind events in the western GOA around Kodiak Island. In both studies, our strategy is to use a combination of observations (satellite data and in situ measurements) and numerical experiments to both document characteristics of gap winds in these regions and to illustrate their influences on the regional oceanography. We treat eastern and western GOA separately because the geographic layout (narrow shelf in the east versus wide shelf in the west), mean ocean circulation (eastern versus western boundary current systems), ecosystem response, and data availability are distinct between these two regions. In Part II (Ladd et al., this issue), we provide a summary comparing across the regions.

2 Methods

2.1 Satellite data

QuikSCAT wind data (downloaded from the NOAA CoastWatch Program http://las.pfeg.noaa.gov/oceanWatch/) were used to quantify the seasonal and interannual frequency of wind events. The SeaWinds instrument, on NASA's QuikSCAT satellite, is a dual-beam microwave scatterometer designed to measure wind magnitude and direction over the global oceans at a reference height of 10 m above the surface with daily coverage of 90% of the earth's oceans. The dataset provided by the CoastWatch Program includes daily averaged winds with 0.25° horizontal resolution. CoastWatch also provides calculations of wind stress curl. All computations, including derivatives, are performed on the individual swath data, which are then mapped to an equal angle grid of 0.25° latitude by 0.25° longitude using a simple arithmetic mean (http://coastwatch.pfeg.noaa.gov/infog/QN_ux10_las.html). QuikSCAT was launched in 1999 and its mission ended in November 2009.

Rain can cause erroneous scatterometer measurements. To ensure complete masking of rain-affected areas, the ultra-conservative Multidimensional Histogram rain-masking algorithm is applied to the wind data (Huddleston and Stiles, 2000). To examine gap winds near Cross Sound, we focused on the region 138.25 – 137°W, 57.5 – 58°N (see Fig. 2 for location of region). We will call this region, the "Cross Sound box". We chose the location of the box > 25 km from the coastline because scatterometer data is contaminated by land within ~25 km of the shoreline (Thompson et al., 2001). To evaluate the influence of missing data due to rain, we examined the number of missing data points in the Cross Sound box. Averaged over the entire time series (1999-2009), the number of missing data points within the box was less than 2%. Data coverage is most limited in August and September when rain is most frequent. However, even in those months, missing data averages less than 4% of the area of the box. QuikSCAT wind speeds are accurate to better than 2 m s^{-1} and wind direction to better than 20°, comparable to *in situ* buoy measurements (Chelton et al., 2004; Freilich and Dunbar, 1999; Vogelzang et al., 2011). Unfortunately, there are no *in situ* wind measurements directly in the path of the Cross Sound gap winds.

The closest National Data Buoy Center buoy is located on the shelf northwest of Cross Sound at 58.237°N, 137.986°W (Fig. 1). Only one year (2003) contained a complete annual cycle of data from the buoy and we used that year for comparison with QuikSCAT winds interpolated to the buoy location (Fig. 3). Correlations between the buoy winds and QuikSCAT winds were significant at over 99.99% confidence (zonal: R = 0.88; meridional R = 0.82). Complex correlation (Kundu, 1976) is independent of the choice of coordinate system and allows estimation of a correlation angle. The complex correlation was also highly significant (R = 0.89) with a correlation angle of -10.5°. The negative correlation angle implies that QuikSCAT winds are rotated clockwise with respect to the buoy winds, but well within the 20° QuikSCAT accuracy found by other investigators (Chelton et al., 2004; Freilich and Dunbar, 1999; Vogelzang et al., 2011).

A Synthetic Aperture Radar (SAR) image from the Alaska SAR Demonstration Project (Young and Winstead, 2004) is shown for comparison with QuikSCAT wind data (Fig. 2). SAR images provide high resolution snapshots of the near-surface wind speed at resolutions of ~100 m to 1 km. However, any given location is imaged less frequently than the scatterometer resulting in limited temporal resolution. The procedures used to generate SAR wind images are described by Monaldo (2000).

Sea surface height anomaly (SSHA) data were downloaded from AVISO (Archiving, Validation and Interpretation of Satellite Oceanographic data; http://www.aviso.altimetry.fr/en/home.html). Trajectories of mesoscale eddies have been derived from AVISO SSHA data by Chelton et. al (2011) using an automated procedure to identify and track eddies with lifetimes > 16 weeks. This dataset was downloaded from http://cioss.coas.oregonstate.edu/eddies/.

Science-quality chlorophyll-a concentration data at the ocean surface from MODIS on the Aqua satellite were downloaded from http://coastwatch.pfeg.noaa.gov. NASA's Goddard Space Flight Center receives the raw satellite data. Processing is accomplished using the SeaWiFS Data Analysis System (SeaDAS) software (Fu et al., 1998; O'Reilly et al., 2000). The chlorophyll-a data are best used for feature identification and tracking. The actual value of chlorophyll-a is somewhat controversial due to major differences when compared with that of the SeaWiFS sensor on Orbview-2. Both can differ substantially from high quality *in situ* measurements.

2.2 Model

The Regional Ocean Modeling System (ROMS) is used to examine the effects of gap-wind events on the regional oceanography. A full description of ROMS can be found in (Haidvogel et al., 2008; Haidvogel et al., 2000; Shchepetkin and McWilliams, 1998; Shchepetkin and McWilliams, 2005), and references therein. The curvilinear horizontal coordinate of ROMS used in this study has a nominal resolution of 3 km and covers the entire GOA. It has 42 generalized terrain-following vertical layers. A multi-year integration of the 3-km GOA ROMS is described in Cheng et al. (2012).

For this study, we compare the results of a “control” experiment and a “gap-wind” experiment. Because the forcing for the gap-wind experiment is based on an event observed in March 2002, both experiments were run from 19 February to 6 May 2002. Both experiments were initialized from the same spun-up state of ROMS from the multi-year integration (Cheng et al., 2012). The lateral boundary conditions for tracer and velocity vector for both experiments are identical and taken from the Simple Ocean Data Assimilation product (SODA, http://iridl.ldeo.columbia.edu/SOURCES/.CARTON-GIESE/.SODA/) version 2, 5-day averages. Additionally, sea surface elevation and currents derived from a tidal model (Foreman et al., 2000) are applied at the open boundaries in both experiments. These tidal signals are allowed to propagate freely throughout the model domain. Four diurnal (O1, Q1, P1, and K1) and four semidiurnal (N2, S2, K2, and M2) tidal constituents are used. In the control experiment, the surface forcing is from the Common Ocean-ice Reference Experiments (CORE, http://data1.gfdl.noaa.gov/nomads/forms/core/COREv2.html), and the forcing variables include daily surface downward longwave and shortwave radiation fluxes, 6-hourly surface air pressure, specific humidity, air temperature, surface wind vectors, and monthly surface precipitation. Surface sensible and latent heat, and momentum fluxes are calculated from the prescribed atmospheric state and modeled sea surface temperature (SST) using bulk aerodynamic formulae (Fairall et al., 1996). Upward longwave radiation flux is also calculated as a function of SST: $LW^{up} = \varepsilon\sigma T^4$ where $\sigma = 5.67 \mathrm{X} 10^{-8}$ W m^{-2} K^{-4} is the Stefan-Boltzmann constant, and ε =0.97 is emissivity of the ocean surface. The horizontal resolution of the CORE forcing is approximately two degrees (~100 km in the GOA), and the forcing variables are interpolated onto the ROMS grid during model integration. In addition to atmospheric forcing, both experiments are driven by monthly freshwater runoff along the Alaskan coast with discharges from the Copper, Alsek, Stikine, Taku, and Susitna Rivers (Royer and Grosch, 2006). The runoff is applied as freshening on the topmost model layer. Total runoff along each segment of coastline is distributed with an exponential taper from the coastal point offshore, with an e-folding scale of 30 km.

Surface forcing in the gap-wind experiment is identical to the control experiment except that an idealized gap-wind event is imposed in the Cross Sound region (Fig. 4). The idealized gap-wind forcing is based on an event observed in March 2002. The maximum QuikSCAT wind speed on 10 March 2002 in the Cross Sound Box was ~25 m s^{-1}. The idealized gap-wind anomaly field was created with maximum wind speed (control run forcing plus gap-wind anomaly) of 25 m s^{-1}, directed from 73°T, and centered at 58°N, 137.35°W. The shape of the anomalous wind patch was created using a two-dimensional elliptical Gaussian function with spatial scales of 1.5° longitude and 0.25° latitude. The anomaly begins on 1 March, peaks on 10 March, and ends on 19 March using a Gaussian function with decay scale of 3 days to simulate the temporal evolution (Fig. 4c). Modeled daily average fields with the tidal signal removed were analyzed.

2.3 Other data

Velocity data from three moorings are used to examine characteristics of the Alaska Coastal Current (and for model comparison) north and south of Cross Sound. These moorings are fully described by Stabeno et al. (this issue-b). Briefly, we use velocities at 25 m depth from SE13 (57.8°N, 136.7°W, south of Cross Sound) and IP1 (58.3°N, 136.9°W, north of Cross Sound) and at 164 m depth from CS4 (58.1 °N, 137.1°W, in Yakobi Sea Valley). Currents at SE13 and IP1 were measured with RCM-9 current meters while those at CS4 were measured with an upward looking 75 kHz acoustic Doppler current profiler.

The Multivariate El Niño Southern Oscillation (ENSO) Index (MEI; Wolter and Timlin, 2011) is used to examine the relationship between ENSO and gap-wind events. This index is downloaded from http://www.esrl.noaa.gov/psd/enso/mei/.

3 Results

3.1 Characteristics of gap-wind events

A wind rose showing the frequency and magnitude of daily average winds (calculated over the entire QuikSCAT record: 21 July 1999 – 21 November 2009) in the Cross Sound box (Fig. 5) indicates that winds are predominantly south-easterly (108 – 144°T) in approximately the along-shore direction. The large-scale coastline near Cross Sound is oriented with an approximate angle of 145/325° from north. To examine only those wind events directed offshore, we selected events with wind direction from between 55 and 85°T. Out of 3747 days of daily-averaged QuikSCAT data, 372 days (~10%) were in the offshore direction (Table 1). Of those, 234 days (63%) recorded maximum daily average wind speed in the Cross Sound box > 10 m s^{-1}. We assume that the events with winds directed offshore and maximum wind speeds > 10 m s^{-1} were gap winds and the focus of the remainder of the paper will be on those 234 events. These events included 59 days with gale force winds (17.5 – 24.7 m s^{-1}), 4 days with storm force winds (24.7 – 32.9 m s^{-1}) and one day with hurricane force winds (> 32.9 m s^{-1} on 15 March 2006). These 64 off-shore directed events accounted for 21% of all days with gale force or stronger winds (>17.5 m s^{-1}) in the Cross Sound box. Note that these speeds come from daily average winds and therefore, higher wind speeds likely occurred over shorter timescales.

A clear seasonal cycle is apparent in the frequency of offshore directed winds (Fig. 6a). Overall, the offshore winds were much more common in the cold months with the highest incidence occurring in March (averaging 5.6 days per month with off-shore winds). Offshore winds with daily speeds < 10 m s^{-1}

were relatively evenly distributed throughout the year while stronger events primarily occurred during the cool season and were almost non-existent during the warm season. Loescher et al. (2006) also noted that wind jet formation originating from offshore directed gap flow is much more likely during the cool season. They note that this seasonality is to be expected as the cool season favors a large contrast between the cold continental interior and the relatively warm offshore waters.

Interannual variability in the number of gap-wind events is also apparent (Fig. 6b). The winter of 2006/2007 had the most events (42), with 14 of those exhibiting average daily wind speeds greater than gale force. The time series of gap wind frequency is significantly correlated with the multivariate ENSO index (MEI; Wolter and Timlin, 2011) implying that gap winds are more common during El Niño years. Including all events with wind speeds > 10 m s^{-1} results in a correlation with the MEI of 0.64 ($p=0.05$) while including only those events with daily average wind speeds greater than gale force results in a correlation of 0.82 ($p=0.004$).

To examine the evolution of a typical event, composites were formed from the events with wind speeds stronger than gale force and separated from each other by more than 7 days (39 events; Fig. 7). These 39 events have an average duration of 3.6 days (Table 2). The maximum duration observed was 12 days for an event in February/March 2007. While the composite winds are strongest in the Cross Sound region, a local wind speed maximum directed offshore is also observed just south of Yakutat Bay suggesting that gap-wind events from Cross Sound and from Yakutat Bay tend to co-occur. The composite offshore wind speed anomaly averaged over the Cross Sound box starts to build about 2 days before the maximum of the composite (Fig. 8). The peak composite offshore wind speed averaged over the region is 12.5 m s^{-1} (after removing the climatological seasonal cycle), more than double the standard deviation. After day 0 of the composite event, winds in the region quickly begin to turn to become southeasterly (Fig. 7). By 3 days post-event, the average wind direction is ~110°T, which is within the most commonly observed directional band (Fig. 5). The region over which composited wind speeds are greater than 10 m s^{-1} extends almost 200 km offshore. The along-shore extent of the high wind region extends almost 225 km along the shelf break (not including the local maximum near Yakutat). Note that the compositing procedure tends to smear the region of high winds. SAR imagery illustrates that gradients in the wind speed at the edges of these events can be very sharp (Fig. 2).

3.2 Effects on surface currents

Using model results we describe the model representation of the regional currents, and examine the influence of a gap-wind event on the circulation. The mean surface flow (averaged over the 76 day control model run) shows the broad, variable Alaska Current over the deep water (> 20 cm s^{-1}) and the Alaska Coastal Current on the continental shelf (Fig. 9). A small (diameter ~ 40 km) anticyclonic eddy centered at 57.25°N, 136.75°W separates the coastal current from the faster current over the deep water. This eddy is smaller than the typical size of a Sitka Eddy (Tabata, 1982) and positioned ~80 km east of its nominal location but may be the model representation of the early formation stages of a Sitka Eddy.

Southeast of Cross Sound, the northwestward flowing coastal current is continuous and relatively stable with most of its variability in the along-shore direction. Velocities measured at 25m from a mooring located at 57.8°N, 136.7°W (SE13, southeast of Cross Sound; Stabeno et al., this issue-b) during 21 March – 7 May 2011 had net velocity ($\bar{u}, \ \bar{v}$) of 9.3 cm s^{-1} with 88% of the variance on the principal axis (330°). Similar directional stability (84% of the variance on a principal axis of 324°) was observed for the same location and time period in 2013. While the model was run for a different year (2002), we compare currents over the same time of year. Model velocities (from the control run) interpolated to the mooring location during 21 March – 7 May show net velocity of 0.7 cm s^{-1} with 98% of the variance on the principal axis (324°).

In the Yakobi Sea Valley directly under the Cross Sound gap winds, velocities measured at 164m during 21 March – 7 May 2011 (CS4 mooring; 58.1°N, 137.1°W) had net velocity of 1.7 cm s^{-1} with 84% of the variance on the principal axis (281°; approximately aligned with the bathymetry of Yakobi Sea Valley). Model velocities interpolated to 164m depth at the CS4 location during 21 March – 7 May show net speed of 0.5 cm s^{-1} with 91% of the variance on the principal axis (218°).

As the coastal current crosses over Yakobi Sea Valley to the wider shelf northwest of Cross Sound, it moves away from the coastline and becomes more variable (Fig. 9). Often, no clearly defined coastal current is evident in the model simulation over this wider shelf. This is consistent with drifter data that show no organized Alaska Coastal Current between Cross Sound and Yakutat Bay (Stabeno et al., this issue-b). Velocities measured at 25m from a mooring located at 58.3°N, 136.9°W (IP1, north of Cross Sound; Stabeno et al., this issue) during 21 March – 7 May 2011 had net velocity of 3.3 cm s^{-1} with 59% of the variance on the principal axis (332°T). Model velocities in this location and time of year show net velocity of 3.6 cm s^{-1} with 93% of the variance on the principal axis (311°T). The net direction of the model current is southeastward (129°T) demonstrating that this location does not typically represent the location of the northwestward coastal current.

A comparison of the control run and the gap-wind forced run illustrates the influence of the gap-wind event on the regional oceanography. In the week after the peak in the wind speed, the average surface current speed at SE13 (south of Cross Sound) in the gap-wind run is 24.7 ± 5.6 cm s^{-1}, significantly faster than in the control run (13.5 ± 4.1 cm s^{-1}). The associated net current direction does not change appreciably between the two runs (327°T in the gap-wind run; 320°T in the control run; approximately oriented along-shore). Surface currents at IP1 (north of Cross Sound) are also significantly faster in the gap-wind case in the week after the peak of the wind event (8.2 ± 2.5 cm s^{-1} vs. 2.8 ± 2.4 cm s^{-1}). In this location the net direction is also affected by the wind event. While the net direction in the absence of the gap-wind event is approximately along-shore (317°T) during the week after the peak in the wind event, in the gap-wind case, the net direction is 176°T (almost due southward). The southward current direction in the gap-wind case is due to an anticyclonic circulation that sets up on the shelf north of the gap-wind axis (Fig. 10).

3.3 Eddies associated with gap winds in observations

The formation of eddies along the eastern boundary of the GOA has been the subject of much recent research (e.g. Combes and Di Lorenzo, 2007; Ladd et al., 2009). Anticyclonic Sitka eddies form south of

Cross Sound near 57°N, 138°W (Tabata, 1982) and Yakutat eddies form along the wider shelf north of Cross Sound (Gower, 1989; Ladd et al., 2005). Mechanisms that may be important to the formation of Sitka eddies include the reflection of atmospherically forced planetary waves (Willmott and Mysak, 1980), interaction between the Alaska Current and the underlying topography (Swaters and Mysak, 1985), and/or abrupt reversals of the prevailing southerly winds (Thomson and Gower, 1998). Many studies have suggested a link between the interannual variability of Sitka eddies and ENSO; downwelling coastal Kelvin waves excited by ENSO (Melsom et al., 1999; Murray et al., 2001) as well as atmospheric teleconnections with the tropics (Melsom et al., 2003; Okkonen et al., 2001) contribute to interannual mesoscale variability in the eastern GOA. Gap winds have been found to be important in the formation of Tehuantepec and Papagayo eddies off the west coast of Central America (e.g. Chang et al., 2012; Liang et al., 2009; McCreary et al., 1989) and may also be important in forcing mesoscale variability in the eastern GOA.

Wind stress curl is negative on the north side of the gap-wind axis and positive on the south side (Fig. 7). Thus, Ekman pumping results in an eddy dipole with an anticyclonic eddy north of the wind axis and a cyclonic eddy south of the axis (Willett et al., 2006). The formation region of the anticyclonic Sitka eddy is south of the Cross Sound gap-wind axis, suggesting that Cross Sound gap-wind events do not contribute to the formation of the Sitka Eddy. However, gap winds from Chatham Strait farther south may play a role in Sitka eddy formation while Cross Sound gap winds may result in formation of Yakutat eddies.

Composites of SSHA (and SST) do not show any significant patterns related to the Cross Sound wind events (not shown). This is not surprising given the high variability in the region, the interaction of multiple closely-spaced gap-wind source regions (Chatham Strait, Cross Sound, Yakutat), and the propagation of eddies into the region. However, a census of eddies (Chelton et al., 2011) suggests that Cross Sound gap winds may be associated with the formation of eddies in the region. An annual time series of the number of eddies formed in January – June of each year in the region 144°W – 134°W; 55°N

– 60°N derived from the Chelton et al. (2011) dataset is significantly correlated with the number of gap-wind events each winter (r = 0.71, p=0.02).

A Sitka eddy and a Yakutat eddy were sampled *in situ* in May 2005 (Ladd et al., 2009). This Sitka eddy was first observed in the altimetry data on 22 December 2004, approximately a week after a gap-wind event was observed flowing from Chatham Strait. The Yakutat eddy was first observed in altimetry data on 23 March 2005. Gap winds were observed flowing from Cross Sound on the 19th and 21st of March 2005. Chlorophyll data from the MODIS satellite (Fig. 11) shows the influence of these two eddies on phytoplankton distributions in the basin. A ribbon of high chlorophyll originating at the coast just north of Chatham Strait appears to be wrapping around the Sitka eddy while high chlorophyll from the region of Cross Sound appears to be wrapping around the Yakutat eddy. *In situ* observations showed high silicate levels in low salinity surface waters at the center of the Yakutat eddy. These high silicate concentrations may indicate riverine input to the core of the eddy (Ladd et al., 2009; Whitney et al., 2005) and may have come from Cross Sound.

3.4 SSH evolution in the model

During spin-up of the gap-wind experiment, surface currents under the wind patch are directed offshore, resulting in coastal upwelling and negative SSHA very near the coast. Sea surface height increases to the north of the wind patch axis and decreases to the south (Fig. 10a) as expected from Ekman convergence/divergence. By 10 March (during peak winds), maximum SSHA absolute value reaches 2 cm. By 16 March (6 days after peak winds), the original SSH anomalies have moved westward off the shelf and maximum SSH anomaly is > 7 cm. Ekman dynamics are still active resulting in continued build-up of positive (negative) SSHA on the shelf to the north (south) of the wind axis (Fig. 10c). By 30 March, 10 days after the end of the gap-wind event, SSHA build-up on the shelf has dissipated, but the SSH anomalies in the ocean basin have persisted and moved westward. The positive anomaly has strengthened to more than 10 cm while the negative anomaly has weakened to < 4 cm.

Throughout the wind event, the SSHA is stronger to the north of the wind event axis (positive SSHA; anticyclonic) than to the south (negative SSHA; cyclonic). Asymmetry in the strength of cyclonic vs. anticyclonic eddies generated by gap winds in the Gulf of Tehuantepec is due to interaction between the Ekman dynamics and entrainment caused by enhanced wind speed (McCreary et al., 1989; Trasviña et al., 1995) and similar processes are acting here. Deeper mixing under the wind jet deepens the pycnocline, enhancing anticyclonic rotation but counteracting cyclonic rotation.

3.5 Modeled effects on surface salinity

While surface salinity anomalies associated with the gap-wind forcing are spatially heterogeneous, some large scale patterns are apparent (Fig. 12). Patches of positive and negative anomalies on the shelf northwest of Cross Sound are associated with the previously mentioned anticyclonic circulation there: positive (negative) salinity anomalies tend to co-locate with the onshore (offshore) circulation anomalies. This result suggests a role of advection in causing such anomalies. Moreover, positive salinity anomalies over Yakobi Sea Valley are due to a combination of entrainment of saltier water from below and enhanced evaporation due to the higher wind speeds. Salinity on a transect oriented across the shelf just southeast of Yakobi Sea Valley shows evidence of upwelling due to the gap-wind event. Isohalines near the coast are raised higher in the water column in the days after the peak of the gap-wind event. Over the course of the event, maximum local surface salinity anomalies on the shelf can reach as high as 0.58. After the gap-wind event, mixed layer salinity on the shelf tends to recover toward mean values exhibited by the control model run.

4 Summary and discussion

Gap-wind events flowing from Cross Sound in the eastern GOA were examined using QuikSCAT wind data. The average duration of an event is 3.6 days with the longest event recorded in the QuikSCAT dataset being 12 days. Daily offshore directed winds with speeds > 10 m s^{-1} are more common during the winter months (October – March) averaging 20.0 days per year (11.0% of winter days), and less common during the summer (April – September) averaging 2.8 days per year (1.5%). Interannual variability in the frequency of gap-wind events is correlated with ENSO. However, the correlation is based on a time series of only 10 years and further study is warranted.

The relationship between ENSO and gap wind frequency could be due to either oceanic or atmospheric processes. El Niño results in warmer surface ocean temperatures in the GOA, resulting in larger contrast between oceanic and continental air masses during the winter. In addition, through atmospheric teleconnections, El Niño influences the sea level pressure field resulting in stronger coastal pressure gradients along the eastern GOA (e.g. Schwing et al., 2002). Both of these influences could result in the higher incidence of gap-wind events observed during El Niño years. Interestingly, gap wind frequency in the western GOA (near Kodiak Island) are not significantly correlated with ENSO (Ladd et al., this issue). This is not unexpected as the influence of ENSO on the GOA is weaker farther north and west.

A composite of 39 gap-wind events in the Cross Sound region illustrates the spatial scales of these events with high off-shore directed winds (> 10 m s^{-1}) reaching almost 200 km off-shore and 225 km along the shelf break. Because the shelf in this region is narrow (20 – 65 km), this suggests that the gap winds directly influence both the shelf and the off-shelf waters.

An ocean circulation model experiment, forced with an idealized gap-wind event, illustrates the effects on the regional ocean. It is important to note that real gap-wind events are highly variable both temporally and spatially. Gap winds are often highly sheared at their edges. In addition, events are not typically stand-alone events. They often build, weaken, and build again over a short period of time. Our idealized model experiment was not designed to reproduce the variety of gap-wind events observed. Rather, we use it to isolate the first-order effects of a generalized gap-wind event on the regional oceanography.

One important finding of the model experiment is that gap winds are likely important to eddy formation in the region. This is suggested by a correlation between the number of gap-wind events and the number of eddies formed each winter from the Chelton et al. (2011) dataset. The model experiment confirms that a gap-wind event can result in eddy formation. An association between El Niño and eddy formation in the eastern GOA has been attributed to both oceanic Kelvin waves propagating from the tropics (Melsom et al., 1999; Murray et al., 2001) and atmospheric teleconnections (Hermann et al., 2009a; Melsom et al., 2003; Okkonen et al., 2001) via the basin scale wind stress curl field. Gap-wind events are more common during El Niño years suggesting that small scale wind events may also play a role in the link between ENSO and eddy formation. Models using lower resolution wind forcing have been shown to form eddies in this region (e.g. Hermann et al., 2009a; Xiu et al., 2012). However, our results suggest that eddy formation in the eastern GOA may be underestimated by models unless model forcing includes high resolution winds that properly account for gap-wind forcing.

Due to influences on circulation, mixing and surface fluxes, in addition to eddy formation, gap winds may influence ecosystem parameters such as larval distribution and transport (Atwood et al., 2010) and nutrient fluxes. The model experiment demonstrates that entrainment of higher salinity water from below the mixed layer is an important result of the gap-wind event on the mixed layer salinity budget. Using salinity/nitrate relationships for the eastern GOA (Ladd et al., 2009), a surface salinity increase of ~0.5 implies that mixed layer nitrate concentrations could increase on the order of 5 – 10 µmole/l, potentially enhancing primary production in the region. This is consistent with a modeling experiment in the northern GOA that found that local wind stress curl is important to upwelling of nitrate on the coastal GOA shelf (Hermann et al., 2009c). We examined satellite chlorophyll data for evidence of gap wind influence. Unfortunately, satellite chlorophyll data in the region is sparse, particularly during the cold season due to low light and frequent extensive cloudiness, and we were not able to confirm effects of gap-wind events on surface chlorophyll concentrations.

Gap-wind events may also result in transport of iron, an important micronutrient, to the surface ocean via dust plumes. Using satellite and meteorological data, Crusius et al. (2011) described dust transport from coastal Alaska into the GOA. They suggested that wind events occurring in autumn, when coastal river levels are low and riverbed sediments are exposed, can transport significant soluble iron to the surface ocean. While our study did not examine the effects of atmospheric dust transport, an influx of iron combined with mixing of nitrate from below could provide highly favorable conditions for primary production.

While our model did not represent the flux of water from Cross Sound, gap winds would likely result in higher flushing of Cross Sound than occurs during periods with calm winds. This enhanced flushing could have important implications for the ecosystems within the sound. The Alaska Coastal Current does not appear to be continuous across the mouth of Cross Sound (Stabeno et al., this issue-b). Our results suggest that the continuity of the Alaska Coastal Current may be variable, with gap-wind events acting to flush Cross Sound, enhance cross-shelf transport, and interrupt the coastal current.

We have shown that one idealized event can spin up eddies and result in changes in circulation and water properties in the regional ocean. In the real world, gap-wind events often occur as a series of events which likely increase the magnitude and duration of the effects on the ocean. The eastern GOA is important for transportation, tourism, and fishing, and high winds can be treacherous to these industries. The influence of these wind events underscores the importance of monitoring winds at high spatial and temporal resolution, particularly near orography.

5 Acknowledgements

QuikSCAT data are produced by Remote Sensing Systems and sponsored by the NASA Ocean Vector Winds Science Team. QuikSCAT wind data were provided by the NOAA CoastWatch Program (http://coastwatch.pfel.noaa.gov) and Remote Sensing Systems, Inc. SAR images were provided by NOAA/NESDIS/STAR and The Johns Hopkins University Applied Physics Laboratory via their website (http://www.star.nesdis.noaa.gov/sod/mecb/sar/index.html). Thanks to William Pichel for information regarding SAR data. MODIS chlorophyll data were obtained from NOAA's CoastWatch Program and NASA's Goddard Space Flight Center, OceanColor Web. NOAA High Resolution SST data provided by the NOAA/OAR/ESRL PSD, Boulder, Colorado, USA, from their Web site at http://www.esrl.noaa.gov/psd/. Comments from Steve Okkonen and two anonymous reviewers led to improvements in the manuscript. Discussions with Phyllis Stabeno, Nick Bond, Sigrid Salo, and Al Hermann are appreciated. This research is contribution EcoFOCI-0815 to NOAA's Ecosystems and Fisheries-Oceanography Coordinated Investigations, PMEL contribution 4112. This publication is partially funded by the Joint Institute for the Study of the Atmosphere and Ocean (JISAO) under NOAA Cooperative Agreement NA10OAR4320148, Contribution 2459. This is GOAIERP publication number 9 and NPRB Publication #562, supported by the North Pacific Research Board through Projects G83 and G84.

6 Figure Captions

Figure 1. Schematic of Gulf of Alaska circulation. Locations of moorings (IP1, CS4, and CS13) and NDBC buoy used for QuikSCAT comparison are noted.

Figure 2. Example of gap-wind event 27 January 2008 from SAR image (left) and QuikSCAT data (right). Wind speed (color; $m\ s^{-1}$) is overlaid with vectors illustrating wind direction. Region used for defining Cross Sound gap-wind events is shown in right panel (white rectangle).

Figure 3. Comparison between QuikSCAT winds (red) and winds observed by NDBC station 46083 Fairweather Ground (black) in 2003.

Figure 4. Wind forcing on 10 March 2002 for (a) Control run, and (b) Gap-wind run. Wind speed (color; $m\ s^{-1}$) is overlaid with wind vectors. White circles denote locations of moorings (IP1, CS4, and CS13) and NDBC buoy (see Fig. 1 for labels). (c) Time amplitude of gap-wind forcing.

Figure 5. Wind rose diagram of daily averaged QuikSCAT wind data in the region 138.25 – 137°W, 57.5 – 58°N illustrating frequency of occurrence in 10 directional and 4 wind speed bins. The plot was created from vector averaged wind direction and maximum wind speed. Wind direction is defined by meteorological convention as the direction from which the winds are blowing.

Figure 6. (a) Monthly histogram of all daily averaged winds averaged over 138.25 – 137°W, 57.5 – 58°N blowing from between 55 and 85°T. (b) Annual histogram of all daily averaged winds with a maximum wind speed in the region of gale force or stronger and blowing from between 55 and 85°T.

Figure 7. Left: Composite of winds derived from 40 gap-wind events separated from each other by more than 7 days and with regional, daily averaged wind speeds greater than gale force (> 17.5 m s^{-1}). Five days are plotted, beginning 2 days before the day of maximum wind speed (Day 0) and ending 2 days after. Wind vectors are overlaid on wind speed (color; m s^{-1}). Right: Windstress curl (N m^{-3}) derived from composite winds on Day 0.

Figure 8. Composite (a) wind speed and (b) wind direction averaged over 138.25 – 137°W, 57.5 – 58°N.

Figure 9. Surface currents averaged over the control model run. Location of 200 m isobath is overlaid (black contour). Locations of three moorings discussed in text are denoted by black circles.

Figure 10. Evolution of sea surface height anomaly (cm) from the model (Gap-wind run – Control run). Plot for 10 March uses a different color bar (top) from the remainder of the plots.

Figure 11. Log MODIS chlorophyll data (8-day composite centered on 6 May 2005) in mg m^{-3}. Contours of 15 cm SSHA from altimetry are overlaid. Schematic arrows (gray) show direction of chlorophyll advection around eddies.

Figure 12. Salinity anomalies (Gap-wind run – Control run) on March 12. Surface current vectors for the gap-wind run are overlaid.

7 Tables

Table 1. Wind events with average wind direction between 55 and 85°T in the region 138.25 – 137°W, 57.5 – 58°N.

Wind speed (m s^{-1})	Number of events	Percentage of total offshore directed events
< 10	138	37
10 – 17.5	170	46
17.5 – 24.7 (gale)	59	16
24.7 – 32.9 (storm)	4	1
> 32.9 (hurricane)	1	0
Total	**372**	**10 (of total days in record)**

Table 2. Duration of 39 events used to form composite (Fig. 7).

Duration	Number of events
≥ 10 days	2
5 – 9 days	10
2 – 4 days	13
1 day	14

8 References

Atwood, E., Duffy-Anderson, J.T., Horne, J.K., Ladd, C., 2010. Influence of mesoscale eddies on ichthyoplankton assemblages in the Gulf of Alaska. Fish. Oceanogr. 19, 493-507. DOI: 10.1111/j.1365-2419.2010.00559.x.

Batchelder, H.P., Bond, N., 2009. Physical and biological patterns, processes and variability in the northeast Pacific. Deep-Sea Res. II 56, 2405-2408. http://dx.doi.org/10.1016/j.dsr2.2009.03.002.

Chang, C.-H., Xie, S.-P., Schneider, N., Qiu, B., Small, J., Zhuang, W., Taguchi, B., Sasaki, H., Lin, X., 2012. East Pacific ocean eddies and their relationship to subseasonal variability in Central American wind jets. J. Geophys. Res. 117, C10001. 10.1029/2011jc007315.

Chelton, D.B., Schlax, M.G., Freilich, M.H., Milliff, R.F., 2004. Satellite measurements reveal persistent small-scale features in ocean winds. Science 303, 978-983. 10.1126/science.1091901.

Chelton, D.B., Schlax, M.G., Samelson, R.M., 2011. Global observations of nonlinear mesoscale eddies. Prog. Oceanogr. 91, 167-216 doi:10.1016/j.pocean.2011.01.002.

Cheng, W., Hermann, A.J., Coyle, K.O., Dobbins, E.L., Kachel, N.B., Stabeno, P.J., 2012. Macro- and micro-nutrient flux to a highly productive submarine bank in the Gulf of Alaska: A model-based analysis of daily and interannual variability. Prog. Oceanogr. 101, 63-77. 10.1016/j.pocean.2012.01.001.

Combes, V., Di Lorenzo, E., 2007. Intrinsic and forced interannual variability of the Gulf of Alaska mesoscale circulation Prog. Oceanogr. 75, 266-286. doi:10.1016/j.pocean.2007.08.011.

Crusius, J., Schroth, A.W., Gassó, S., Moy, C.M., Levy, R.C., Gatica, M., 2011. Glacial flour dust storms in the Gulf of Alaska: Hydrologic and meteorological controls and their importance as a source of bioavailable iron. Geophys. Res. Lett. 38, L06602. 10.1029/2010gl046573.

Fairall, C.W., Bradley, E.F., Rogers, D.P., Edson, J.B., Young, G.S., 1996. Bulk parameterization of air-sea fluxes for Tropical Ocean-Global Atmosphere Coupled-Ocean Atmosphere Response Experiment. Journal of Geophysical Research: Oceans 101, 3747-3764. 10.1029/95JC03205.

Foreman, M.G.G., Crawford, W.R., Cherniawsky, J.Y., Henry, R.F., Tarbotton, M.R., 2000. A high-resolution assimilating tidal model for the northeast Pacific Ocean. J. Geophys. Res. - Oceans 105, 28629-28651.

Freilich, M.H., Dunbar, R.S., 1999. The accuracy of the NSCAT 1 vector winds: Comparisons with National Data Buoy Center buoys. J. Geophys. Res. 104, 11231-11246. 10.1029/1998jc900091.

Fu, G., Baith, K.S., McClain, C.R., 1998. SeaDAS: The SeaWiFS Data Analysis System. Proceedings of The 4th Pacific Ocean Remote Sensing Conference, Qingdao, China, 73-79.

Gower, J.F.R., 1989. Geosat altimeter observations of the distribution and movement of sea-surface height anomalies in the north-east Pacific, Oceans 89: The Global Ocean. Institute of Electrical and Electronics Engineers, Seattle, Washington, 977-981 p.

Haidvogel, D.B., Arango, H.G., Budgell, W.P., Cornuelle, B.D., Curchitser, E.N., Di Lorenzo, E., Fennel, K., Geyer, W.R., Hermann, A.J., Lanerolle, L., Levin, J., McWilliams, J.C., Miller, A.J., Moore, A.M., Powell, T.M., Shchepetkin, A.G., Sherwood, C.R., Signell, R.P., Warner, J.C., Wilkin, J., 2008. Ocean forecasting in terrain-following coordinates: Formulation and skill assessment of the Regional Ocean Modeling System. Journal of Computational Physics 227, 3595-3624.

Haidvogel, D.B., Arango, H.G., Hedstrom, K., Beckmann, A., Malanotte-Rizzoli, P., Shchepetkin, A.G., 2000. Model evaluation experiments in the North Atlantic Basin: simulations in nonlinear terrain-following coordinates. Dyn. Atmos. Ocean. 32, 239-281.

Hermann, A.J., Curchitser, E.N., Haidvogel, D.B., Dobbins, E.L., 2009a. A comparison of remote vs local influence of El Niño on the coastal circulation of the northeast Pacific. Deep-Sea Res. II 56, 2427-2443. doi:10.1016/j.dsr2.2009.02.005.

Hermann, A.J., Hinckley, S., Dobbins, E.L., Haidvogel, D.B., Bond, N.A., Mordy, C., Kachel, N., Stabeno, P.J., 2009c. Quantifying cross-shelf and vertical nutrient flux in the Coastal Gulf of Alaska with a spatially nested, coupled biophysical model. Deep-Sea Res. II 56, 2474-2486. doi:10.1016/j.dsr2.2009.02.008.

Huddleston, J.N., Stiles, B.W., 2000. Multidimensional Histogram (MUDH) Rain Flag Product Description, Version 2.1., Jet Propulsion Laboratory, Pasadena, CA, p.

Janout, M.A., Weingartner, T.J., Okkonen, S.R., Whitledge, T.E., Musgrave, D.L., 2009. Some characteristics of Yakutat Eddies propagating along the continental slope of the northern Gulf of Alaska. Deep-Sea Res. II 56, 2444-2459. doi:10.1016/j.dsr2.2009.02.006.

Kessler, W.S., 2006. The circulation of the eastern tropical Pacific: A review. Prog. Oceanogr. 69, 181-217.
Kowalik, Z., Luick, J.L., Royer, T.C., 1994. On the dynamics of the Alaska Coastal Current. Cont. Shelf Res. 14, 831-845.
Kundu, P.K., 1976. Ekman veering observed near the ocean bottom. J. Phys. Oceanogr. 6, 238-242.
Ladd, C., Cheng, W., Salo, S., this issue. Gap Winds and their effects on regional oceanography Part II: Kodiak Island, Alaska. Deep-Sea Res. II.
Ladd, C., Crawford, W.R., Harpold, C.E., Johnson, W.K., Kachel, N.B., Stabeno, P.J., Whitney, F., 2009. A synoptic survey of young mesoscale eddies in the Eastern Gulf of Alaska. Deep-Sea Res. II 56, 2460–2473. doi:10.1016/j.dsr2.2009.02.007.
Ladd, C., Kachel, N.B., Mordy, C.W., Stabeno, P.J., 2005. Observations from a Yakutat eddy in the northern Gulf of Alaska. J. Geophys. Res. - Oceans 110, C03003. doi: 10.1029/2004JC002710.
Ladd, C., Mordy, C.W., Kachel, N.B., Stabeno, P.J., 2007. Northern Gulf of Alaska eddies and associated anomalies. Deep-Sea Res. I 54, 487-509. doi:10.1016/j.dsr.2007.01.006.
Liang, J.-H., McWilliams, J.C., Gruber, N., 2009. High-frequency response of the ocean to mountain gap winds in the northeastern tropical Pacific. J. Geophys. Res. - Oceans 114. C12005, doi:10.1029/2009JC005370.
Liu, H., Olsson, P.Q., Volz, K.P., Yi, H., 2006. A climatology of mesoscale model simulated low-level wind jets over Cook Inlet and Shelikof Strait, Alaska. Estuarine, Coastal and Shelf Science 70, 551-566. 10.1016/j.ecss.2006.06.011.
Liu, H.B., Olsson, P.Q., Volz, K., 2008. SAR observation and modeling of gap winds in the Prince William Sound of Alaska. Sensors 8, 4894-4914. 10.3390/s8084894.
Loescher, K.A., Young, G.S., Colle, B.A., Winstead, N.S., 2006. Climatology of barrier jets along the Alaskan coast. Part 1: Spatial and temporal distributions. Mon. Wea. Rev. 134, 437-453.
Macklin, S.A., Lackmann, G.M., Gray, J., 1988. Offshore-directed winds in the vicinity of Prince William Sound, Alaska. Mon. Wea. Rev. 116, 1289-1301.
McClain, C.R., Christian, J.R., Signorini, S.R., Lewis, M.R., Asanuma, I., Turk, D., Dupouy-Douchement, C., 2002. Satellite ocean-color observations of the tropical Pacific Ocean. Deep-Sea Res. II 49, 2533-2560. doi: 10.1016/s0967-0645(02)00047-4.
McCreary, J.P., Lee, H.S., Enfield, D.B., 1989. The response of the coastal ocean to strong offshore winds: With application to circulations in the Gulfs of Tehuantepec and Papagayo. J. Mar. Res. 47, 81-109.
Melsom, A., Metzger, E.J., Hurlburt, H.E., 2003. Impact of remote oceanic forcing on Gulf of Alaska sea levels and mesoscale circulation. J. Geophys. Res. - Oceans 108, 3346. doi:10.1029/2002JC001742.
Melsom, A., Meyers, S.D., Hurlburt, H.E., Metzger, J.E., O'Brien, J.J., 1999. ENSO effects on Gulf of Alaska eddies. Earth Interactions 3, 1-30.
Monaldo, F.M., 2000. The Alaska SAR demonstration and near-real-time synthetic aperture radar winds, Johns Hopkins APL Technical Digest, 75-79 p.
Murray, C.P., Morey, S.L., O'Brien, J.J., 2001. Interannual variability of upper ocean vorticity balances in the Gulf of Alaska. J. Geophys. Res. - Oceans 106, 4479-4491.
O'Reilly, J.E., Maritorena, S., Siegel, D.A., O'Brien, M.C., Toole, D., Chavez, F.P., Strutton, P., G.F. Cota, S.B. Hooker, C.R. McClain, K.L. Carder, F. Muller-Karger, L. Harding, A. Magnuson, D. Phinney, G.F. Moore, J. Aiken, K.R. Arrigo, R. Letelier, Culver, M., 2000. Ocean Chlorophyll a Algorithms for SeaWiFS, OC2, and OC4: Version 4. In: O'Reilly, J.E., 24 Coauthors (Eds.), SeaWiFS Postlaunch Calibration and Validation Analyses, Part 3, NASA Tech. Memo. 2000-206892. NASA Goddard Space Flight Center, Greenbelt, MD, pp. 9-19.
Okkonen, S.R., Jacobs, G.A., Metzger, E.J., Hurlburt, H.E., Shriver, J.F., 2001. Mesoscale variability in the boundary currents of the Alaska Gyre. Cont. Shelf Res. 21, 1219-1236.
Okkonen, S.R., Weingartner, T.J., Danielson, S.L., Musgrave, D.L., Schmidt, G.M., 2003. Satellite and hydrographic observations of eddy-induced shelf-slope exchange in the northwestern Gulf of Alaska. J. Geophys. Res. 108, 3033. doi:10.1029/2002JC001342.

Reed, T.R., 1931. Gap winds of the Strait of Juan de Fuca. Mon. Wea. Rev. 59, 373-376. 10.1175/1520-0493(1931)59<373:gwotso>2.0.co;2.

Rodionov, S.N., Bond, N.A., Overland, J.E., 2007. The Aleutian Low, storm tracks, and winter climate variability in the Bering Sea. Deep-Sea Res. II 54, 2560-2577.

Rodionov, S.N., Overland, J.E., Bond, N.A., 2005. Spatial and temporal variability of the Aleutian climate. Fish. Oceanogr. 14, 3-21. doi:10.1111/j.1365-2419.2005.00363.x.

Royer, T.C., 1981. Baroclinic transport in the Gulf of Alaska Part II. A fresh-water driven coastal current. J. Mar. Res. 39, 251-266.

Royer, T.C., Grosch, C.E., 2006. Update of a freshwater discharge model for the Gulf of Alaska, North Pacific Research Board Final Report 734, 12 p.

Schumacher, J.D., Reed, R.K., 1986. On the Alaska Coastal Current in the Western Gulf of Alaska. J. Geophys. Res. - Oceans 91, 9655-9661.

Schwing, F.B., Murphree, T., deWitt, L., Green, P.M., 2002. The evolution of oceanic and atmospheric anomalies in the northeast Pacific during the El Niño and La Niña events of 1995–2001. Prog. Oceanogr. 54, 459-491. http://dx.doi.org/10.1016/S0079-6611(02)00064-2.

Shchepetkin, A.F., McWilliams, J.C., 1998. Quasi-Monotone Advection Schemes Based on Explicit Locally Adaptive Dissipation. Mon. Wea. Rev. 126, 1541-1580. 10.1175/1520-0493(1998)126<1541:QMASBO>2.0.CO;2.

Shchepetkin, A.G., McWilliams, J.C., 2005. The Regional Ocean Modeling System (ROMS): A split-explicit, free-surface, topography-following coordinates ocean model. Ocean Modelling 9, 347-404.

Stabeno, P., Bond, N.A., Hermann, A.J., Kachel, N.B., Mordy, C.W., Overland, J.E., 2004. Meteorology and oceanography of the northern Gulf of Alaska. Cont. Shelf Res. 24, 859-897.

Stabeno, P.J., Bell, S., Cheng, W., Danielson, S., Kachel, N.B., Mordy, C.W., this issue-a. Long-term observations of Alaska Coastal Current in the northern Gulf of Alaska. Deep-Sea Res. II.

Stabeno, P.J., Bond, N.A., Kachel, N.B., Ladd, C., Mordy, C., Strom, S.L., this issue-b. Southeast Alaska: Currents, mixing and chlorophyll-a. Deep-Sea Res. II.

Swaters, G.E., Mysak, L.A., 1985. Topographically-induced baroclinic eddies near a coastline, with application to the Northeast Pacific. J. Phys. Oceanogr. 15, 1470-1485.

Tabata, S., 1982. The anticyclonic, baroclinic eddy off Sitka, Alaska, in the northeast Pacific Ocean. J. Phys. Oceanogr. 12, 1260-1282.

Thompson, D.R., Monaldo, F.M., Beal, R.C., Winstead, N.S., Pichel, W.G., Clemente-Colón, P., 2001. Combined estimates improve high-resolution coastal wind mapping. Eos, Transactions American Geophysical Union 82, 469-474. 10.1029/01EO00278.

Thomson, R.E., Gower, J.F.R., 1998. A basin-scale oceanic instability event in the Gulf of Alaska. J. Geophys. Res. 103, 3033-3040.

Trasviña, A., Barton, E.D., Brown, J., Velez, H.S., Kosro, P.M., Smith, R.L., 1995. Offshore wind forcing in the Gulf of Tehuantepec, Mexico: The asymmetric circulation. J. Geophys. Res. 100, 20649-20663. doi: 10.1029/95jc01283.

Vogelzang, J., Stoffelen, A., Verhoef, A., Figa-Saldana, J., 2011. On the quality of high-resolution scatterometer winds. J. Geophys. Res. - Oceans 116. 10.1029/2010jc006640.

Weingartner, T., Eisner, L., Eckert, G.L., Danielson, S., 2009. Southeast Alaska: oceanographic habitats and linkages. J. Biogeogr. 36, 387-400. doi:10.1111/j.1365-2699.2008.01994.x.

Whitney, F.A., Crawford, D.W., Yoshimura, T., 2005. The uptake and export of silicon and nitrogen in HNLC waters of the NE Pacific Ocean. Deep-Sea Res. II 52, 1055-1067.

Willett, C.S., Leben, R.R., Lavin, M.F., 2006. Eddies and Tropical Instability Waves in the eastern tropical Pacific: A review. Prog. Oceanogr. 69, 218-238.

Willmott, A.J., Mysak, L.A., 1980. Atmospherically forced eddies in the Northeast Pacific. J. Phys. Oceanogr. 10, 1769-1791.

Wilson, J.G., Overland, J.E., 1986. Meteorology. In: Hood, D.W., Zimmerman, S.T. (Eds.), The Gulf of Alaska, Physical Environment and Biological Resources. U.S. Department of Commerce, National

Oceanic and Atmospheric Administration, National Ocean Service, Office of Oceanography and Marine Assessment, Ocean Assessments Division, Alaska Office p. 655.

Winstead, N.S., Colle, B.A., Bond, N.A., Young, G., Olson, J., Loescher, K., Monaldo, F., Thompson, D., Pichel, W., 2006. Using SAR remote sensing, field observations, and models to better understand coastal flows in the Gulf of Alaska. Bull. Amer. Meteor. Soc. 87, 787–800

Wolter, K., Timlin, M.S., 2011. El Niño/Southern Oscillation behaviour since 1871 as diagnosed in an extended multivariate ENSO index (MEI.ext). International Journal of Climatology 31, 1074-1087. 10.1002/joc.2336.

Xiu, P., Chai, F., Xue, H., Shi, L., Chao, Y., 2012. Modeling the mesoscale eddy field in the Gulf of Alaska. Deep-Sea Res. I 63, 102-117. http://dx.doi.org/10.1016/j.dsr.2012.01.006.

Young, G., Winstead, N., 2004. Meteorological phenomena in high resolution SAR wind imagery, in: Beal, B., Young, G., Monaldo, F., Thompson, D., Winstead, N., Scott, C. (Eds.), High Resolution Wind Monitoring with Wide Swath SAR: A User's Guide, 13-31 p.

9 Web References

AVISO, http://www.aviso.altimetry.fr/en/home.html, last accessed April 2015.

Chelton, D.B. and Schlax, M.G., Mesoscale eddies in altimeter observations of SSH. http://cioss.coas.oregonstate.edu/eddies/, last accessed July 2013.

Common Ocean-ice Reference Experiments (CORE), http://data1.gfdl.noaa.gov/nomads/forms/core/COREv2.html, last accessed April 2012.

NOAA CoastWatch Program webpage, http://las.pfeg.noaa.gov/oceanWatch/, last accessed April 2015.

NOAA Coastwatch QuikSCAT webpage, http://coastwatch.pfeg.noaa.gov/infog/QN_ux10_las.html, last accessed April 2015.

NOAA Coastwatch MODIS/Aqua webpage, http://coastwatch.pfeg.noaa.gov/infog/MB_chla_las.html, accessed April 2015.

Simple Ocean Data Assimilation product (SODA, http://iridl.ldeo.columbia.edu/SOURCES/.CARTON-GIESE/.SODA/), last accessed April 2012.

Multivariate El Niño Southern Oscillation (ENSO) Index, http://www.esrl.noaa.gov/psd/enso/mei/, last accessed April 2015.

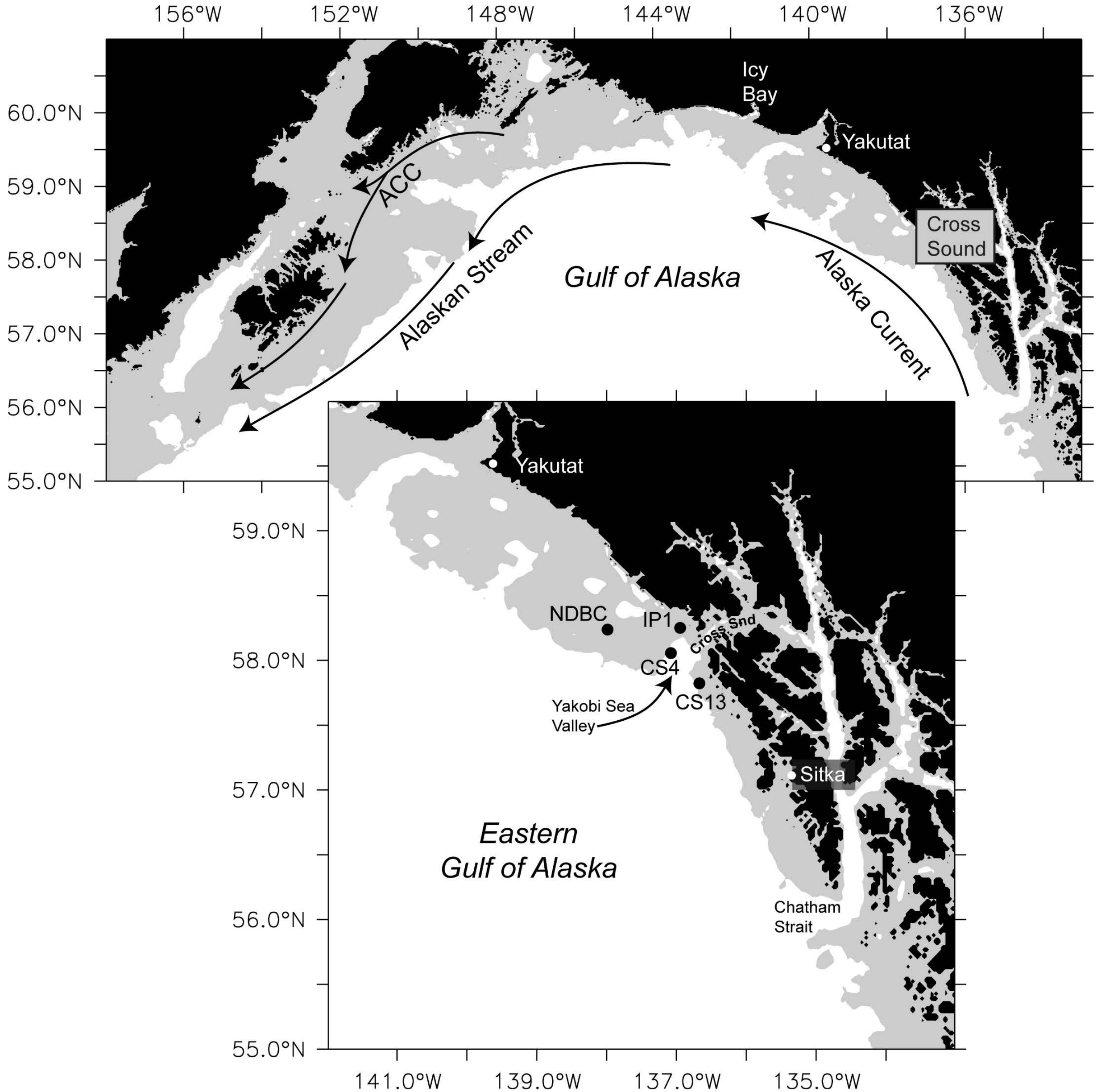
156°W
152°W
148°W
144°W
140°W
136°W
60.0°N
59.0°N
58.0°N
57.0°N
56.0°N
55.0°N
Icy Bay
Yakutat
ACC
Alaskan Stream
Gulf of Alaska
Alaska Current
Cross Sound
Yakutat
59.0°N
58.0°N
57.0°N
56.0°N
55.0°N
NDBC
IP1
Cross Snd
CS4
CS13
Yakobi Sea Valley
Sitka
Eastern Gulf of Alaska
Chatham Strait
141.0°W
139.0°W
137.0°W
135.0°W

Fig. 1

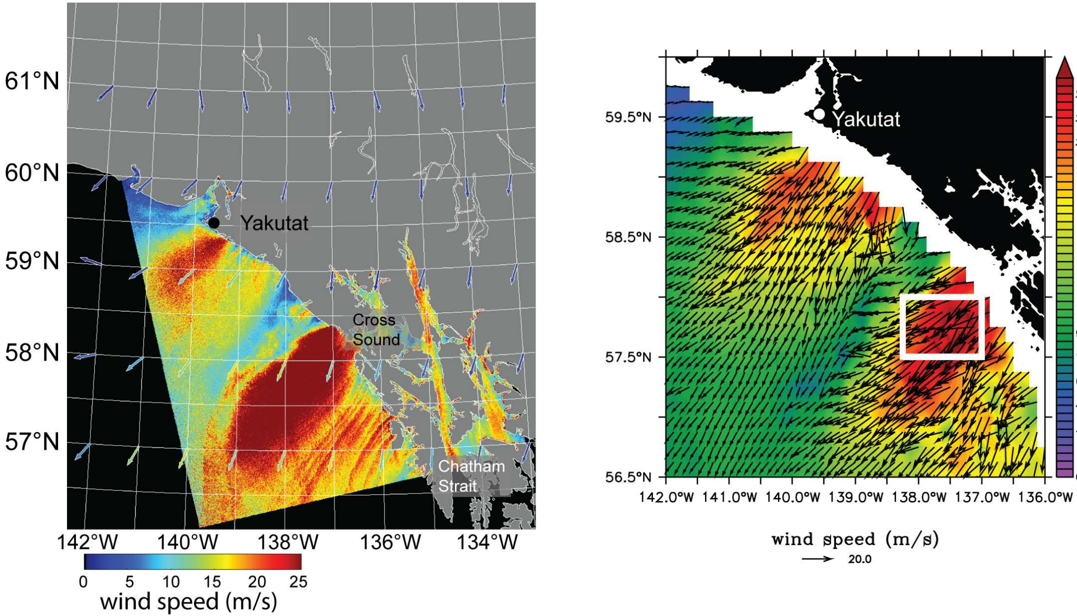
61°N
60°N
59°N
58°N
57°N
Yakutat
Cross Sound
Chatham Strait
142°W
140°W
138°W
136°W
134°W
0
5
10
15
20
25
wind speed (m/s)
59.5°N
58.5°N
57.5°N
56.5°N
142.0°W
141.0°W
140.0°W
139.0°W
138.0°W
137.0°W
136.0°W
24
22.5
21
19.5
18
16.5
15
13.5
12
10.5
9
7.5
6
4.5
3
1.5
0
wind speed (m/s)
20.0

Fig. 2

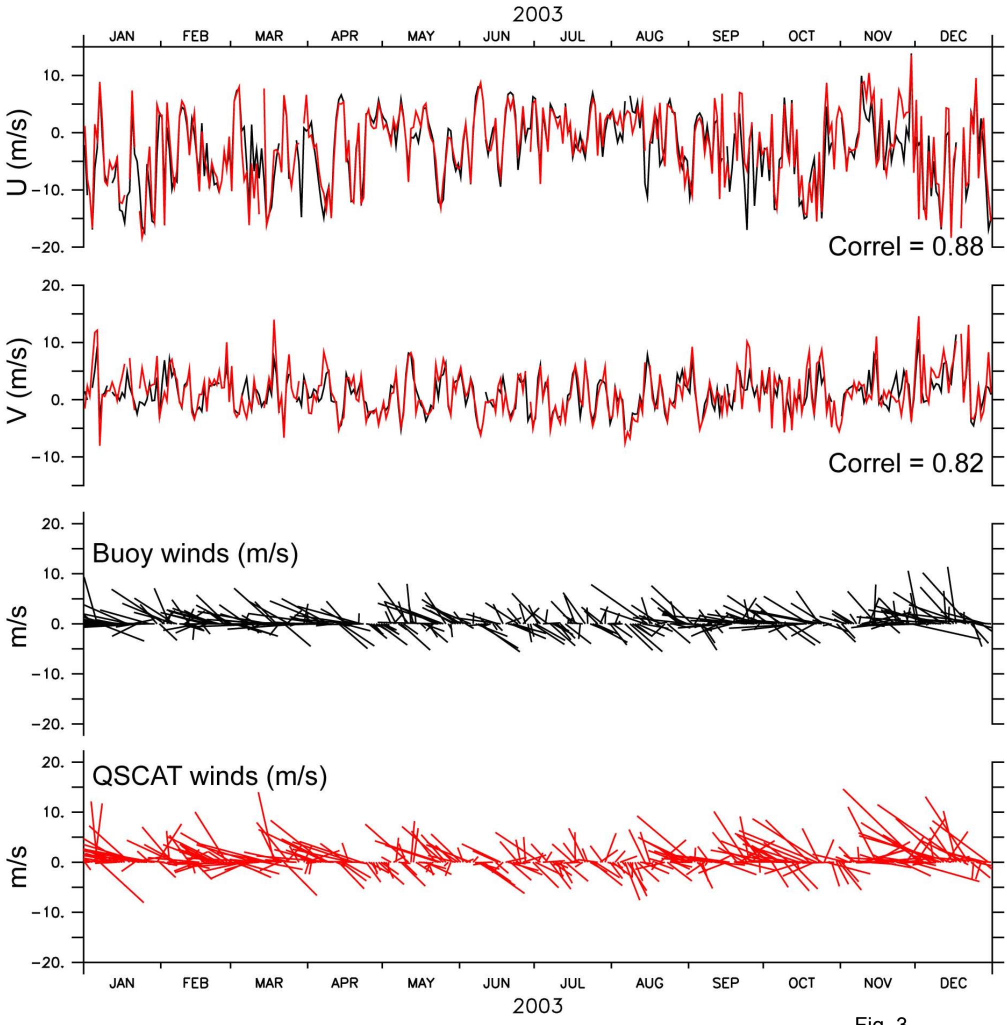

2003
JAN
FEB
MAR
APR
MAY
JUN
JUL
AUG
SEP
OCT
NOV
DEC
U (m/s)
10.
0.
−10.
−20.
Correl = 0.88
V (m/s)
20.
10.
0.
−10.
Correl = 0.82
Buoy winds (m/s)
m/s
20.
10.
0.
−10.
−20.
QSCAT winds (m/s)
m/s
20.
10.
0.
−10.
−20.
JAN
FEB
MAR
APR
MAY
JUN
JUL
AUG
SEP
OCT
NOV
DEC
2003

Fig. 3

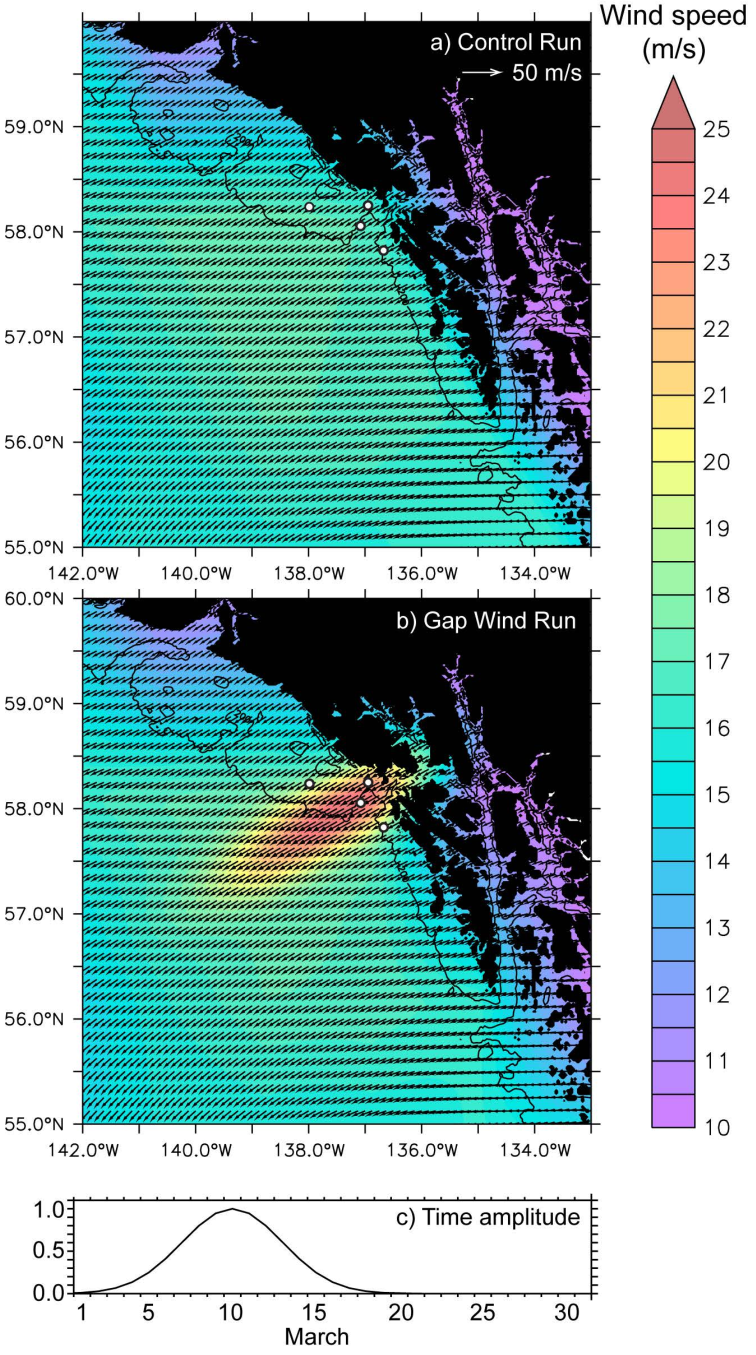
Wind speed (m/s)
a) Control Run
50 m/s
b) Gap Wind Run
c) Time amplitude
March
59.0°N
58.0°N
57.0°N
56.0°N
55.0°N
60.0°N
142.0°W
140.0°W
138.0°W
136.0°W
134.0°W
10
11
12
13
14
15
16
17
18
19
20
21
22
23
24
25
1.0
0.5
0.0
1
5
10
15
20
25
30

Fig. 4

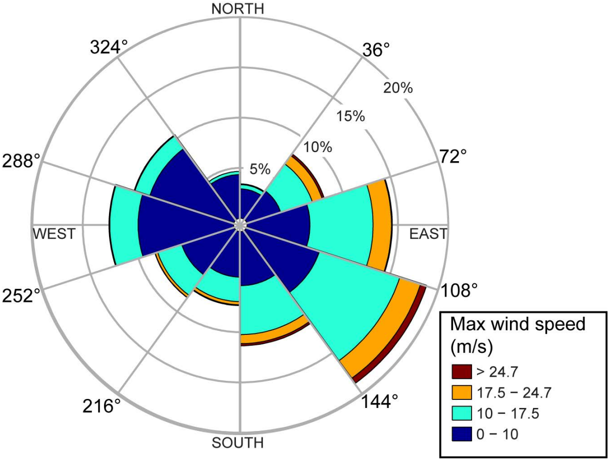

NORTH
36°
72°
EAST
108°
144°
SOUTH
216°
252°
WEST
288°
324°
5%
10%
15%
20%
Max wind speed (m/s)
> 24.7
17.5 − 24.7
10 − 17.5
0 − 10

Fig. 5

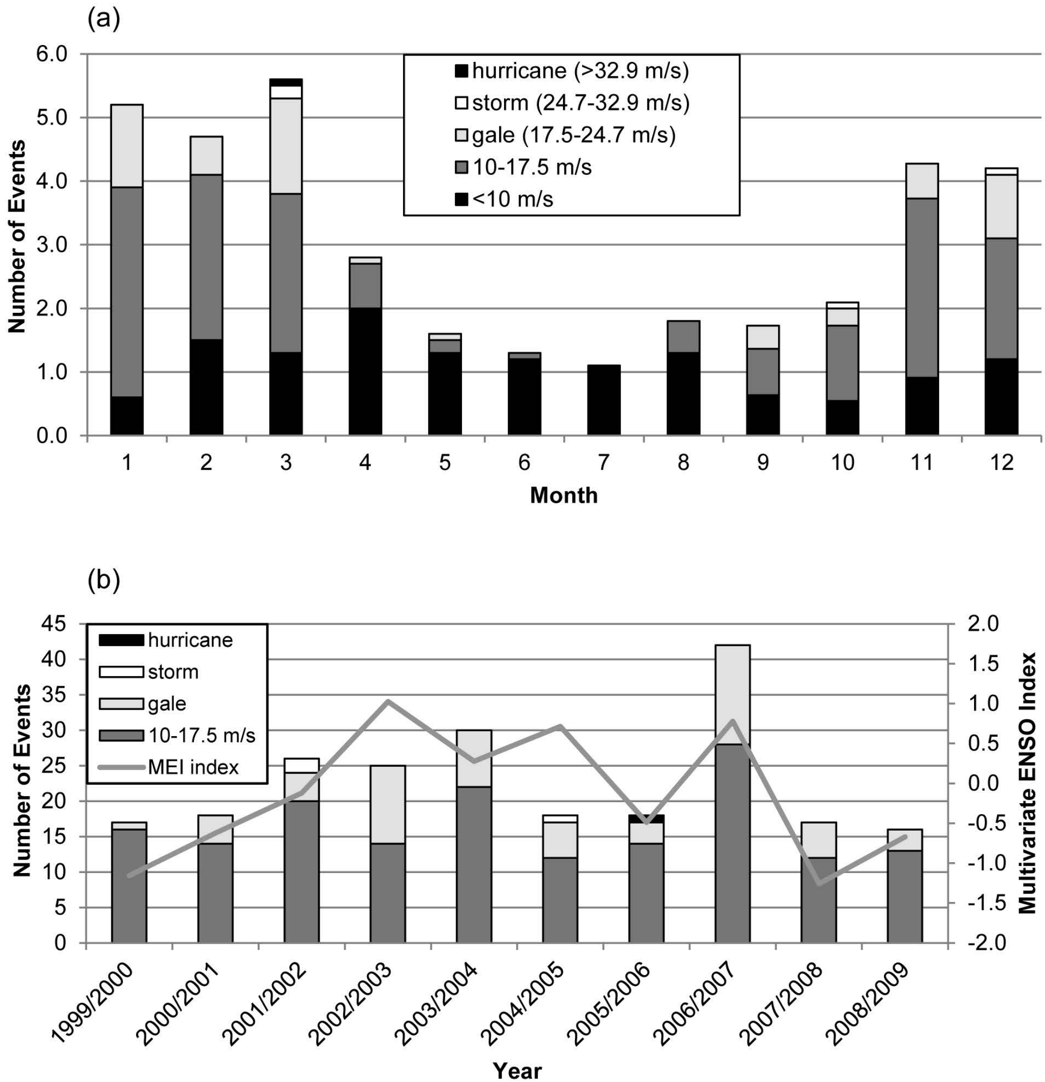
(a)
hurricane (>32.9 m/s)
storm (24.7-32.9 m/s)
gale (17.5-24.7 m/s)
10-17.5 m/s
<10 m/s
Number of Events
6.0
5.0
4.0
3.0
2.0
1.0
0.0
1
2
3
4
5
6
7
8
9
10
11
12
Month
(b)
hurricane
storm
gale
10-17.5 m/s
MEI index
Number of Events
45
40
35
30
25
20
15
10
5
0
Multivariate ENSO Index
2.0
1.5
1.0
0.5
0.0
-0.5
-1.0
-1.5
-2.0
1999/2000
2000/2001
2001/2002
2002/2003
2003/2004
2004/2005
2005/2006
2006/2007
2007/2008
2008/2009
Year

Fig. 6

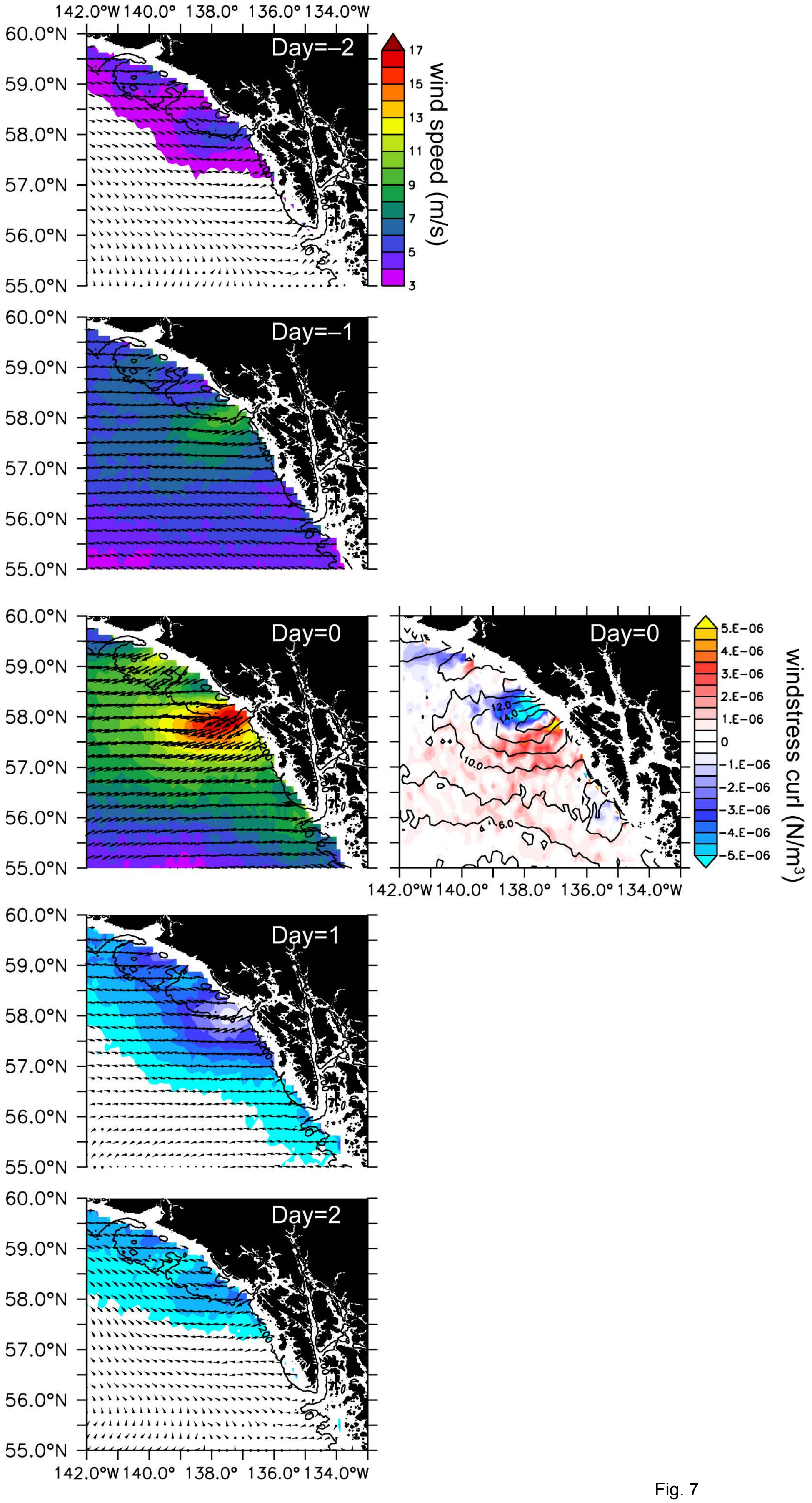

142.0°W 140.0° 138.0° 136.0° 134.0°W
60.0°N
59.0°N
58.0°N
57.0°N
56.0°N
55.0°N
Day=–2
Day=–1
Day=0
Day=1
Day=2
wind speed (m/s)
3
5
7
9
11
13
15
17
windstress curl (N/m^3)
5.E-06
4.E-06
3.E-06
2.E-06
1.E-06
0
-1.E-06
-2.E-06
-3.E-06
-4.E-06
-5.E-06
12.0
14.0
10.0
6.0

Fig. 7

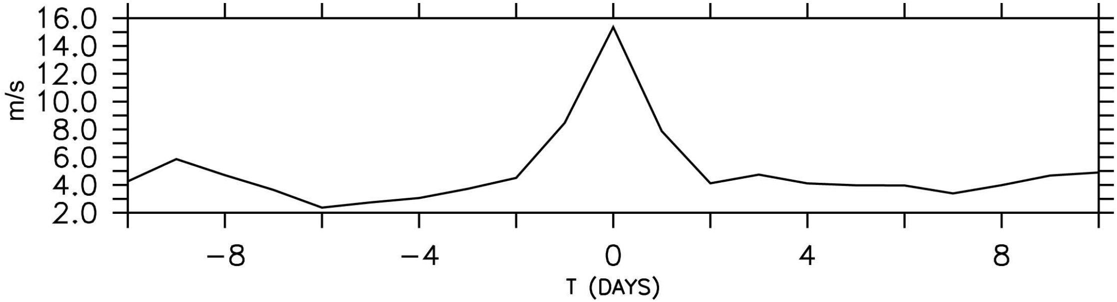

Composite wind speed (m/s)

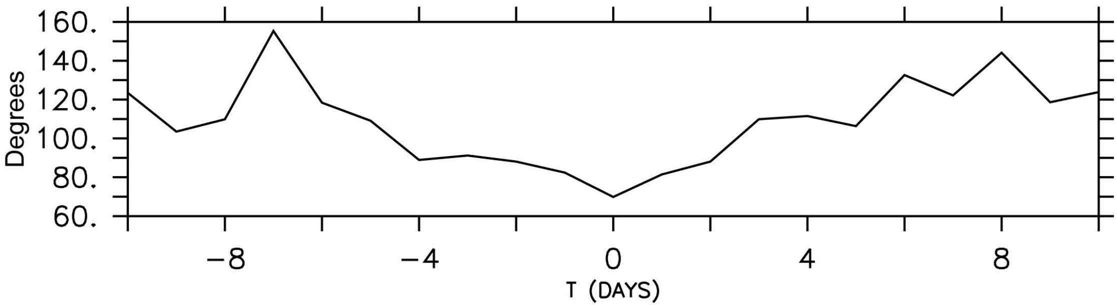

Composite wind direction (deg)

Fig. 8

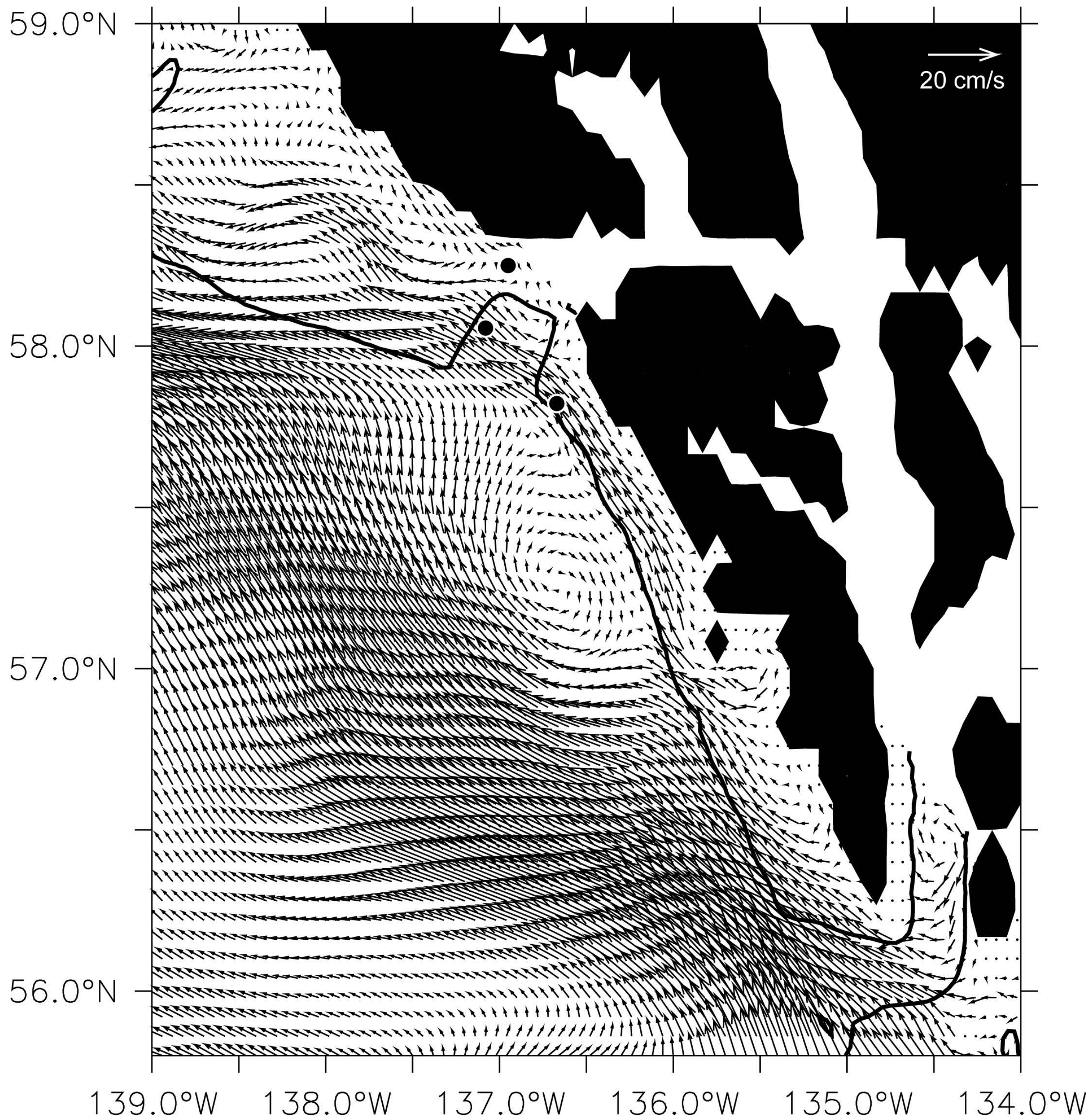
59.0°N
58.0°N
57.0°N
56.0°N
139.0°W
138.0°W
137.0°W
136.0°W
135.0°W
134.0°W
20 cm/s

Fig. 9

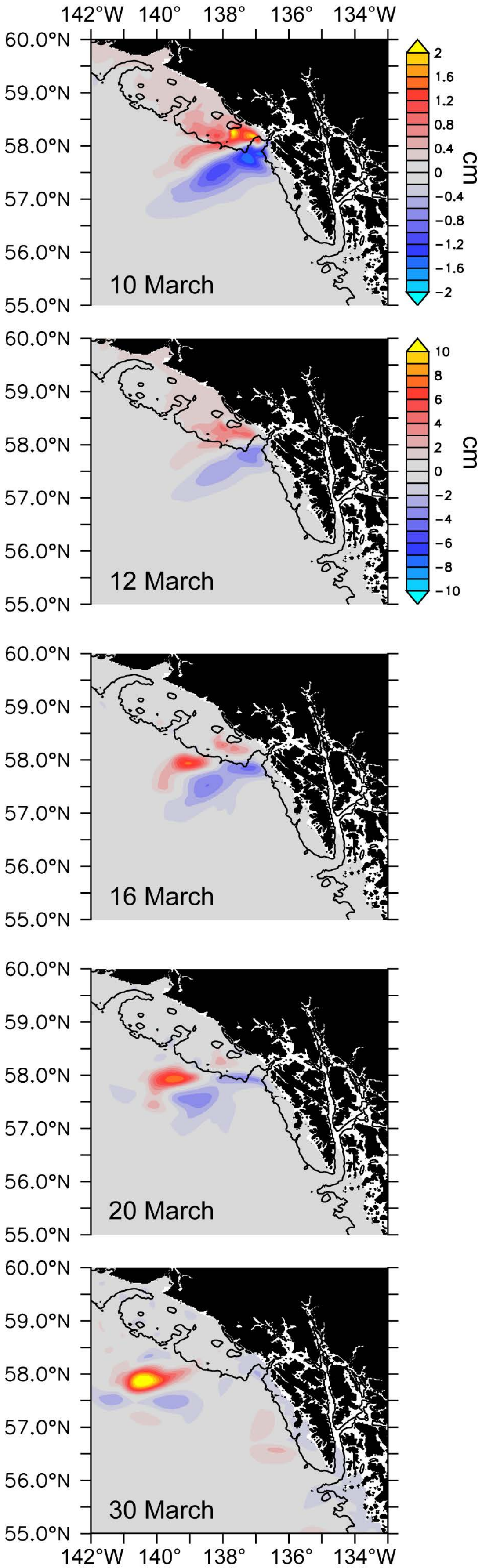
142°W
140°
138°
136°
134°W
60.0°N
59.0°N
58.0°N
57.0°N
56.0°N
55.0°N
10 March
2
1.6
1.2
0.8
0.4
0
−0.4
−0.8
−1.2
−1.6
−2
cm
12 March
10
8
6
4
2
0
−2
−4
−6
−8
−10
cm
16 March
20 March
30 March

Fig. 10

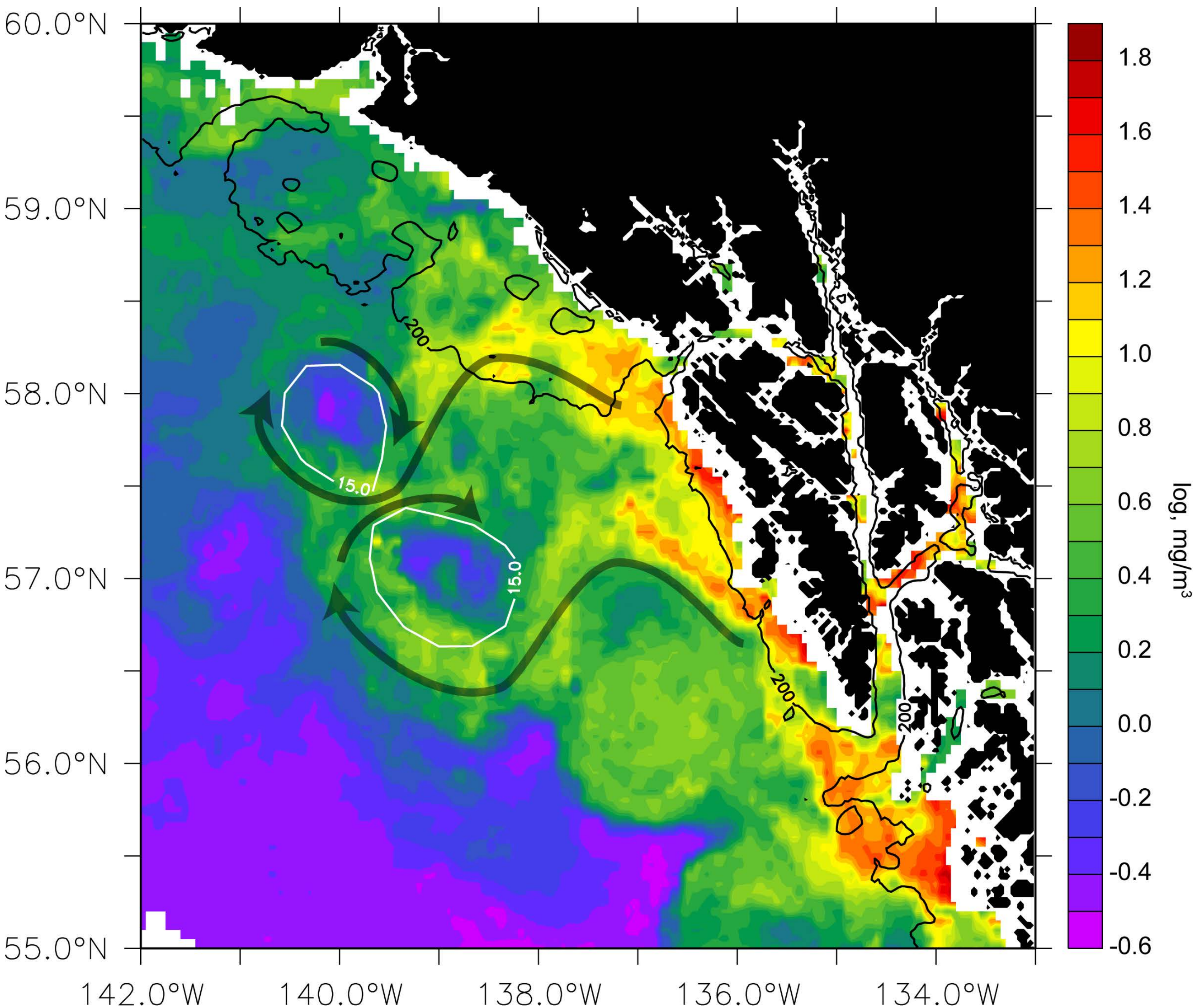

60.0°N
59.0°N
58.0°N
57.0°N
56.0°N
55.0°N
142.0°W
140.0°W
138.0°W
136.0°W
134.0°W
200
200
200
15.0
15.0
1.8
1.6
1.4
1.2
1.0
0.8
0.6
0.4
0.2
0.0
-0.2
-0.4
-0.6
log, mg/m3

Fig. 11

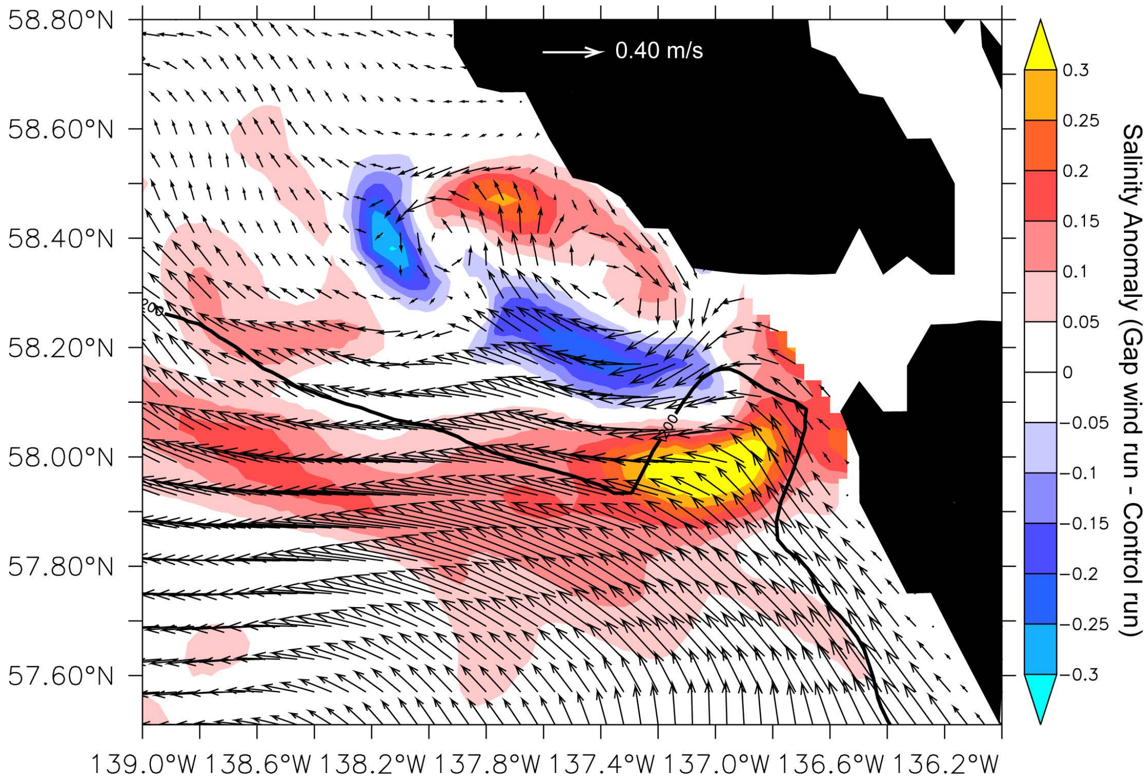
0.40 m/s
58.80°N
58.60°N
58.40°N
58.20°N
58.00°N
57.80°N
57.60°N
139.0°W
138.6°W
138.2°W
137.8°W
137.4°W
137.0°W
136.6°W
136.2°W
200
0.3
0.25
0.2
0.15
0.1
0.05
0
−0.05
−0.1
−0.15
−0.2
−0.25
−0.3
Salinity Anomaly (Gap wind run - Control run)

Fig. 12